



**HAL**  
open science

# Surface free energy calculation of the solid–fluid interfaces from molecular simulation

Aziz Ghoufi

► **To cite this version:**

Aziz Ghoufi. Surface free energy calculation of the solid–fluid interfaces from molecular simulation. *AIP Advances*, 2024, 14 (4), <10.1063/5.0188578>. <hal-04567366>

**HAL Id: hal-04567366**

**<https://hal.science/hal-04567366v1>**

Submitted on 3 May 2024

**HAL** is a multi-disciplinary open access archive for the deposit and dissemination of scientific research documents, whether they are published or not. The documents may come from teaching and research institutions in France or abroad, or from public or private research centers.


L'archive ouverte pluridisciplinaire **HAL**, est destinée au dépôt et à la diffusion de documents scientifiques de niveau recherche, publiés ou non, émanant des établissements d'enseignement et de recherche français ou étrangers, des laboratoires publics ou privés.



HAL Authorization

RESEARCH ARTICLE | APRIL 09 2024

# Surface free energy calculation of the solid–fluid interfaces from molecular simulation

Aziz Ghoufi  


 Check for updates

AIP Advances 14, 045116 (2024)


<https://doi.org/10.1063/5.0188578>



03 May 2024 09:19:49



**Biomicrofluidics**  
Special Topic:  
Microfluidic Biosensors  
**Submit Today**



# Surface free energy calculation of the solid–fluid interfaces from molecular simulation

Cite as: AIP Advances 14, 045116 (2024); doi: 10.1063/5.0188578

Submitted: 22 November 2023 • Accepted: 19 March 2024 •

Published Online: 9 April 2024



View Online



Export Citation



CrossMark

Aziz Ghoufi<sup>a)</sup>

## AFFILIATIONS

Univ Paris-East Creteil, CNRS, ICMPE (UMR 7182), 2 rue Henri Dunant, Thiais F-94320, France and Institut de Physique de Rennes, IPR, CNRS-Université de Rennes 1, UMR CNRS 6251, 35042 Rennes, France

<sup>a)</sup> Author to whom correspondence should be addressed: [aziz.ghoufi@u-pec.fr](mailto:aziz.ghoufi@u-pec.fr) and [aziz.ghoufi@univ-rennes1.fr](mailto:aziz.ghoufi@univ-rennes1.fr)

## ABSTRACT

In this work, I present a straightforward approach for computing surface free energy  $\gamma_F$  based on the assessment of surface internal energy ( $\gamma_U$ ), avoiding the difficulty connected to the determination of the elastic contribution in the case of a solid surface. This methodology has thus been extended to the calculation of  $\gamma_F$  for the interface between the liquid–vapor phase of water, the solid–vapor interface of aluminum, the aluminum–water interface, rigid graphene–water solid–liquid interfaces, and the *n*-dodecane–water liquid–liquid interface.

© 2024 Author(s). All article content, except where otherwise noted, is licensed under a Creative Commons Attribution (CC BY) license (<https://creativecommons.org/licenses/by/4.0/>). <https://doi.org/10.1063/5.0188578>

## I. INTRODUCTION

Understanding the distinctions among surface tension, interfacial energy, interfacial tension, surface energy, surface free energy, and surface stress often leads to confusion. Surface stress, also referred to as interfacial tension or surface tension ( $\tau$ ), denotes the reversible work per unit area required to elastically stretch an existing surface, inherently involving elasticity concepts.<sup>1</sup> It is represented as a tensor ( $\tau_{ij}$ ) and is associated with the resistance against surface deformation, originating from forces acting at the material's surface. In contrast, surface free energy, interfacial energy, or simply surface energy ( $\gamma$ ) can be defined as the useable work attainable from an isothermal, isobaric thermodynamic, or closed system, respectively.<sup>2,3</sup> These quantities are scalar. ( $\gamma$ ) quantifies the disruption of intermolecular bonds occurring upon the creation of a surface, whereas ( $\tau_{ij}$ ) only considers elastic deformation without involving bond breakage.

While surface tension (ST) and surface free energy (SFE) (the terms used in this work to denote both contributions) are commonly mistaken for being identical, they are not precisely the same. In the case of liquids, the interfacial energy remains constant even as the surface is stretched, which results in similarities between surface tension and interfacial energy. However, for solids, these two contributions diverge due to alterations in the atomic structure of the solid surface during elastic deformation.

The calculation of liquid–vapor surface free energy is now well-established and can be determined through both mechanical and thermodynamic approaches utilizing the tensor pressure<sup>4</sup> and the energy response resulting from surface perturbation,<sup>5–7</sup> respectively. Over the past three decades, extensive theoretical and numerical efforts have been dedicated to its assessment, and Ref. 8 offers a pertinent review of its computation. In contrast, evaluating the surface free energy for solid–liquid and solid–vapor interfaces is more challenging due to the elastic contribution, as highlighted by Shuttleworth's relation<sup>9</sup> [Eq. (1)]. Here,  $\gamma$ ,  $\tau_{ij}$ , and  $\epsilon_{ij}$  represent the surface free energy, surface stress along the *i* and *j* directions, and deformation along the *i* and *j* axes, respectively,

$$\tau_{ij} = \gamma + \frac{\partial \gamma}{\partial \epsilon_{ij}}. \quad (1)$$

In the normal direction of the solid surface (*z* axis), the surface stress ( $\tau_{zz}$ ) is zero while the constraint ( $\sigma_{zz}$ ) is constant due to mechanical equilibrium, while  $\tau_{xx} = \tau_{yy}$  owing to the symmetry of the surface in a tetragonal reference. Here,  $\tau = (\tau_{xx} + \tau_{yy})/2$  corresponds to the surface tension. Under these conditions, the Shuttleworth relation can be reformulated as follows:

$$\tau = \gamma + \frac{\partial \gamma}{\partial \epsilon}. \quad (2)$$

If the solid is rigid or if the interface corresponds to the liquid–vapor or liquid–liquid interfaces, the elasticity contribution is zero, and  $\gamma = \tau$ . This explains why SFE and ST are often used interchangeably. While the first term of Eqs. (1) and (2), i.e.,  $\tau$ , can be easily calculated from the constraint tensor, the main difficulty in predicting the SFE of a solid surface lies in the fact that  $\frac{\partial \gamma}{\partial \epsilon}$  cannot be calculated. However, it is possible to overcome this problem by using the cleaving method,<sup>10–17</sup> a thermodynamic perturbation method. This approach involves cleaving a unified solid into two separated volumes using a perturbation of van der Waals interactions with a coupling parameter.<sup>15</sup> By evaluating the energy difference between both perturbed and unperturbed states within the same statistical ensemble, the term  $\frac{\partial \gamma}{\partial \epsilon}$  vanishes, so the free energy difference corresponds to the term  $\gamma$ . This approach has been successfully employed to calculate the SFE of solid–vapor interfaces<sup>15</sup> and solid–liquid interfaces.<sup>17</sup> Furthermore, Di Pasquale and Davidchack utilized this methodology to evaluate  $\frac{\partial \gamma}{\partial \epsilon}$  using the cleaving method as a function of strain  $\epsilon$  to demonstrate the validity of Shuttleworth’s relation.<sup>15</sup> Although this method is robust, it requires very long simulations (more than a hundred states of 10–20 ns to achieve converged surface tension) and necessitates the use of fictive (perturbed) states. Interestingly, at absolute 0 K, the entropic term is zero and, therefore, the surface free energy corresponds to the surface internal energy given by

$$\gamma = \gamma_U - T\gamma_S \text{ with } \gamma_S = 0 \text{ at } T = 0 \text{ K,} \quad (3)$$

where  $\gamma_U$  and  $\gamma_S$  represent the surface internal energy and surface entropy, respectively. By considering the cleaving of a unified bulk solid (designated as  $u$ ) into two separate solids (designated as  $s$ ),  $\gamma_U$  can be calculated based on the transformation depicted in Fig. 1. In this scenario, the surface free energy corresponds to the work ( $W$ ) required for the cleaving process, which thermodynamically equates to the free energy difference between the initial and final states, i.e.,  $W = \Delta F$ , leading to Eq. (4). From a statistical mechanics perspective, internal energy ( $U$ ) is connected to the configurational energy ( $\mathcal{U}$ ) obtained from molecular simulation,

$$\gamma = \frac{W}{2A} = \frac{\Delta F}{2A} = \frac{F_s - F_u}{2A} \sim \frac{U_s - U_u}{2A} = \frac{\mathcal{U}_s - \mathcal{U}_u}{2A} \text{ at } T = 0 \text{ K.} \quad (4)$$

The factor of 1/2 accounts for the presence of two interfaces. At temperatures other than 0 K, the surface free energy cannot be rigorously assessed from Eq. (4) because the entropic terms for both the separated and unified solids are indeterminate. However, these entropic terms can be approximated by considering the evaporation heat of an adsorbed gas monolayer on the surface.<sup>18</sup>

Benjamin and Horbach have also developed a method to compute the crystal–liquid interfacial free energy via thermodynamic integration, requiring several perturbation windows.<sup>19</sup> More recently, Wu and Firoozabadi derived working expressions for estimating solid–fluid interfacial free energy based on the free-energy perturbation method with consideration of solid deformation.<sup>20</sup> Their results reveal that the contribution of solid deformation highly depends on the stress conditions in the solid, which can be either positive or negative. Similar to the cleaving method, this approach requires performing several simulations for different solid deformations. This approach was recently criticized by Chapman and

Asthaigiri, claiming an incorrect formulation of the first law of thermodynamics for a solid–liquid system.<sup>21</sup> Addula and Punathanam,<sup>22</sup> and more recently, Yeandel and co-workers,<sup>23</sup> have also developed a new method to extract solid/liquid interfacial free energies from molecular simulation using the perturbation method. The common point of all these methods is the perturbation method based on thermodynamic integration or free energy perturbation, which requires the trajectory to be divided into several thermodynamic sub-states.<sup>13,14,18–24</sup>

To sum up, both primitive and perturbation cleaving methods, as well as the application of Shuttleworth’s relation for SFE calculation at finite temperatures, are either inconsistent or computationally expensive. In this work, I offer an approach to determine surface free energy by calculating the excess surface internal energy and studying its temperature dependence, which enables the prediction of surface entropy.

## II. SURFACE FREE ENERGY CALCULATION

### A. Theoretical framework

For an interfacial system involving a phase with elasticity, the differential of the surface internal energy ( $U^*$ ) or excess internal energy can be expressed as

$$dU^* = TdS^* + \gamma dA + \sum_i \mu_i dN_i^* + \sum_{ij} \left[ \delta \epsilon_{ij}^{\parallel} \tau_{ij} + \sigma_{ij}^{\perp} \delta_{ij} \right] A, \quad (5)$$

where  $\epsilon_{ij}^{\parallel}$ ,  $\sigma_{ij}^{\perp}$ ,  $e_{ij}$ ,  $\tau_{ij}$ , and  $\delta_{ij}$  represent the parallel strain, normal stress, interfacial excess quantity of the parallel components of the bulk stress tensor, and interfacial excess quantity of the perpendicular components of the bulk strain tensor, respectively.  $S^*$  is the excess entropy related to the interfacial one,  $N_i^*$  is the excess amount of  $i$ , and  $\mu_i$  is the chemical potential of  $i$ . This relation is derived from the application of the first thermodynamic principle, taking into account both the interface term ( $\gamma dA$ ) and the elasticity term ( $[\delta \epsilon_{ij}^{\parallel} \tau_{ij} + \sigma_{ij}^{\perp} \delta_{ij}] A$ ), which can be equated to an elastic work. Through the use of the Euler equation, it becomes possible to obtain the excess internal energy,

$$U^* = TS^* + \gamma A + \sum_i \mu_i N_i^*. \quad (6)$$

The excess free energy ( $F^*$ ) can then be expressed as follows:

$$F^* = U^* - TS^* = \gamma A + \sum_i \mu_i N_i^*. \quad (7)$$

From this, I can introduce the generalized grand potential,

$$\Omega^* = F^* - \sum_i \mu_i N_i^* = \gamma A. \quad (8)$$

Equation (8) demonstrates that  $\gamma$  is connected to the surface grand potential. Similarly to  $U^*$ , after simplification, the differential of  $F^*$  can be expressed as

$$dF^* = -S^* dT + \gamma dA + \sum_i \mu_i dN_i^* + \sum_{ij} \left[ \delta \epsilon_{ij}^{\parallel} \tau_{ij} + \sigma_{ij}^{\perp} \delta_{ij} \right] A. \quad (9)$$

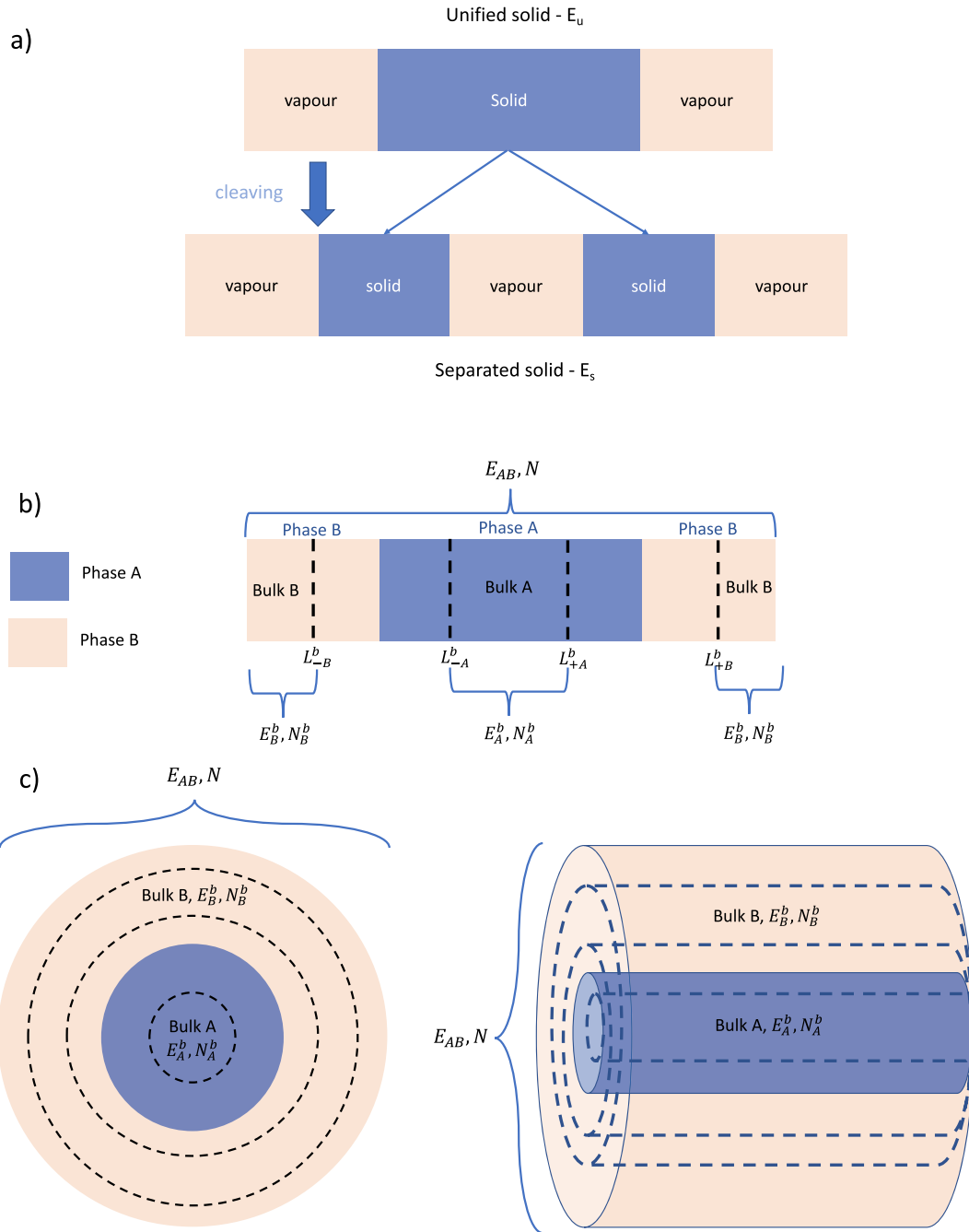


**FIG. 1.** (a) Illustration of the method for calculating the surface free energy at 0 K using both unified energy ( $E_u$ ) and separated energy ( $E_s$ ) with Eq. (4). (b) Illustration of the different regions considered in the calculation of surface internal energy between two phases, A and B [Eq. (5)]. Here,  $E_{AB}$ ,  $E_A^b$ ,  $E_B^b$ ,  $N_A^b$ ,  $N_B^b$ ,  $N_A$ ,  $N_B$ , and  $N$  represent the total energy, the energy of B in the bulk phase, the energy of A in the bulk phase, the number of molecules of A in the bulk phase, the number of molecules of B in the bulk phase, the total number of molecules A, the total number of molecules B, and the total number of A and B molecules, respectively.  $L_-^b$  and  $L_+^b$  denote the limits of the bulk regions. (c) Similar representation to part (b) for spherical and cylindrical interfaces.

03 May 2024 09:19:49

By using Eq. (7), it is possible to establish a relation between surface free energy ( $\gamma_F = \frac{F^*}{A}$ ), internal energy ( $\gamma_U = \frac{U^*}{A}$ ), and entropy ( $\gamma_S = \frac{S^*}{A}$ ),

$$\gamma_F = \gamma_U - T\gamma_S = \frac{F^*}{A} \rightarrow F^* = \gamma_F A = \gamma A + \sum_i \mu_i N_i^*, \quad (10)$$

which entails the relation

$$\gamma = \gamma_F - \sum_i \mu_i \Gamma_i^* \quad \text{such as } \Gamma_i^* = \frac{N_i^*}{A}. \quad (11)$$

$\Gamma_i^*$  is the surface excess concentration of component  $i$ . Henceforth, the surface free energy will be denoted as  $\gamma_F$ , directly linked to the free energy ( $F^*$ ), while  $\gamma$  will be associated with the grand potential ( $\Omega^*$ ). Consequently, I opt to designate  $\gamma$  as the surface grand potential to distinguish it from SFE. Equation (9) yields the subsequent set of partial derivative equations

$$\begin{aligned} \gamma &= \left( \frac{\partial F^*}{\partial A} \right)_{T, N_i^*, \epsilon_{ij}^{\parallel}, \sigma_{ij}^{\perp}} = \left( \frac{\partial [\gamma_F A]}{\partial A} \right)_{T, N_i^*, \epsilon_{ij}^{\parallel}, \sigma_{ij}^{\perp}} \\ &= \gamma_F + A \left( \frac{\partial \gamma_F}{\partial A} \right)_{T, N_i^*, \epsilon_{ij}^{\parallel}, \sigma_{ij}^{\perp}}, \end{aligned} \quad (12)$$

$$\begin{aligned} S^* &= - \left( \frac{\partial F^*}{\partial T} \right)_{A, N_i^*, \epsilon_{ij}^{\parallel}, \sigma_{ij}^{\perp}} = - \left( \frac{\partial [\gamma_F A]}{\partial T} \right)_{A, N_i^*, \epsilon_{ij}^{\parallel}, \sigma_{ij}^{\perp}} \\ &= -A \left( \frac{\partial \gamma_F}{\partial T} \right)_{A, N_i^*, \epsilon_{ij}^{\parallel}, \sigma_{ij}^{\perp}} - \gamma_F \left( \frac{\partial A}{\partial T} \right)_{A, N_i^*, \epsilon_{ij}^{\parallel}, \sigma_{ij}^{\perp}}. \end{aligned} \quad (13)$$

The last term of Eq. (13) is zero, as the surface area is constant. Finally, I obtain

$$\gamma_S = - \left( \frac{\partial \gamma_F}{\partial T} \right)_{A, N_i^*, \epsilon_{ij}^{\parallel}, \sigma_{ij}^{\perp}}. \quad (14)$$

Very interestingly, the equation obtained, Eq. (12), bears a striking resemblance to the one derived by Dong, which establishes a connection between differential and integral surface free energy.<sup>25</sup> By comparing with the work of Dong, one can equate  $\gamma_F$  with the integrated surface tension of Gibbs surface tension, which is sensitive to the surface area. The last term of Eq. (12) ( $\left( \frac{\partial \gamma_F}{\partial A} \right)_{T, N_i^*, \epsilon_{ij}^{\parallel}, \sigma_{ij}^{\perp}}$ ) cannot be calculated directly, as it requires a perturbation of surface area while keeping  $\epsilon_{ij}^{\parallel}, \sigma_{ij}^{\perp}$  constant, which is not feasible. However, by comparing Eqs. (11) and (12), one can derive Eq. (15), which allows for the calculation of this derivative,

$$A \left( \frac{\partial \gamma_F}{\partial A} \right)_{T, N_i^*, \epsilon_{ij}^{\parallel}, \sigma_{ij}^{\perp}} = - \sum_i \mu_i \Gamma_i^*. \quad (15)$$

Additionally, by differentiating  $F^*$  [the last term of Eq. (10)] and comparing it with Eq. (9), I obtain the following expression:

$$d\gamma = -\gamma_S dT - \sum_i d\mu_i \Gamma_i + \sum_{ij} \left[ \delta \epsilon_{ij}^{\parallel} (\tau_{ij} - \gamma \delta_{ij}) + \sigma_{ij}^{\perp} \delta_{ij} \right], \quad (16)$$

and

$$d\gamma_F = -\gamma_S dT + \sum_i d\Gamma_i \mu_i + \sum_{ij} \left[ \delta \epsilon_{ij}^{\parallel} (\tau_{ij} - \gamma \delta_{ij}) + \sigma_{ij}^{\perp} \delta_{ij} \right], \quad (17)$$

where  $\delta_{ij}$  denotes the Kronecker delta. Equation (16) is derived by considering a reversible transformation that involves both deformation (at a constant number of atoms) and creation (at a constant strain) of the surface. In this case, the excess internal energy must account for both the work of creation,  $\gamma dA^{\text{cre}}$ , and the work of deformation. This leads to  $dA^{\text{cre}} = dA - A \delta \epsilon_{ij}^{\parallel} \delta_{ij}$ . Upon equating Eqs. (16) and (17) with the partial derivatives, I obtain

$$\gamma_S = - \left( \frac{\partial \gamma}{\partial T} \right)_{\mu_i, \epsilon_{ij}^{\parallel}, \sigma_{ij}^{\perp}} = - \left( \frac{\partial \gamma_F}{\partial T} \right)_{N_i, \epsilon_{ij}^{\parallel}, \sigma_{ij}^{\perp}}, \quad (18)$$

$$\tau_{ij} - \gamma \delta_{ij} = A \left( \frac{\partial \gamma}{\partial \epsilon_{ij}^{\parallel}} \right)_{T, \mu_i, \sigma_{ij}^{\perp}} = A \left( \frac{\partial \gamma_F}{\partial \epsilon_{ij}^{\parallel}} \right)_{T, N_i, \sigma_{ij}^{\perp}}. \quad (19)$$

Very interestingly, Eq. (19) corresponds to Shuttleworth's relation [Eq. (1)], while Eq. (18) enables the calculation of the interfacial entropy from  $\gamma$  and  $\gamma_F$ . However,  $\gamma_S$  can only be calculated from  $\gamma_F$  in the canonical or  $N_p n A T$  statistical ensembles. Indeed,  $\gamma$  has to be evaluated in the grand canonical ensemble where  $\mu_i$  of each type of molecule is kept constant.

## B. SFE ( $\gamma_F$ ) calculation from SIE ( $\gamma_U$ )

While the entropic term is challenging to calculate,  $\gamma_U$  can be computed using the following relation:  $\gamma_U = \frac{U^*}{A}$ , allowing  $U^*$  to be directly evaluated from the configurational energy ( $\mathcal{U}$ ) obtained from molecular simulations.<sup>26,27</sup> To do this, two phases (A and B) must be divided into two regions, as highlighted in Fig. 1(b). Similar to  $\gamma_U$ , surface tension can be calculated from the excess contribution of the constraint tensor ( $\sigma_{\alpha\beta}$ ),<sup>26,27</sup>

$$\gamma_U = \frac{\mathcal{U}^*}{A} = \frac{\mathcal{U}_{AB} - N_A \cdot \mathcal{U}_A^b / N_A^b - N_B \cdot \mathcal{U}_B^b / N_B^b}{A}, \quad (20)$$

$$\tau_{\alpha\beta} = \frac{\sigma_{\alpha\beta}^*}{A} = \frac{\sigma_{\alpha\beta} - N_A \cdot \sigma_{\alpha\beta, A}^b / N_A^b - N_B \cdot \sigma_{\alpha\beta, B}^b / N_B^b}{A}, \quad (21)$$

where  $\mathcal{U}_{AB}$ ,  $\mathcal{U}_A^b$ ,  $\mathcal{U}_B^b$ ,  $N_A^b$ ,  $N_B^b$ ,  $N_A$ ,  $N_B$ , and  $N$  are the total energy, the energy of B in the bulk phase, the energy of A in the bulk phase, the number of molecules of A in the bulk phase, the number of molecules of B in the bulk phase, the total number of molecules of A, the total number of molecules of B, and  $N$  is the total number of A and B molecules, respectively.  $\sigma$  represents the constraint component in the  $\alpha$  and  $\beta$  directions. Importantly, Eq. (20) can be applied regardless of the physical nature of the interface [Liquid-Vapor (LV), Solid-Liquid (SL), or Solid-Vapor (SV)] or its shape (cylindrical, spherical, or planar), as shown in Figs. 1(b) and 1(c). It is, therefore, sufficient to determine the limits of both bulk regions from the zones where the profiles of the density of the centers of mass of the molecules are constant. Furthermore, it is necessary to be sufficiently far from the interfacial region, which requires boxes along the normal of the interface that are long enough.  $\mathcal{U}_A^b$  and  $\mathcal{U}_B^b$

can be calculated from the local energy ( $U(z)$ ) of a slab located at  $z$ , such as

$$U(z) = \sum_i^N \sum_{j \neq i}^N (U_{ij} \cdot H(z_i)) / 2, \text{ with } U^b = \sum_{z=L_-^b}^{z=L_+^b} U(z), \quad (22)$$

with  $L_-^b$   $L_+^b$  representing the limits of the bulk regions, as illustrated in Fig. 1(b). As demonstrated earlier, the surface free energy can be expressed as

$$\gamma_F = \gamma_U - T\gamma_S. \quad (23)$$

If I differentiate this relation with respect to temperature, I obtain the following equation:

$$\left(\frac{\partial \gamma_F}{\partial T}\right)_{A, N_i^*, \epsilon_{ij}^{\parallel}, \sigma_{ij}^{\perp}} = \left(\frac{\partial \gamma_U}{\partial T}\right)_{A, N_i^*, \epsilon_{ij}^{\parallel}, \sigma_{ij}^{\perp}} - \gamma_S - T \left(\frac{\partial \gamma_S}{\partial T}\right)_{A, N_i^*, \epsilon_{ij}^{\parallel}, \sigma_{ij}^{\perp}}. \quad (24)$$

As shown in Eq. (18),  $\left(\frac{\partial \gamma_U}{\partial T}\right)_{A, N_i^*, \epsilon_{ij}^{\parallel}, \sigma_{ij}^{\perp}} = -\gamma_S$ , which simplifies Eq. (24) to

$$\left(\frac{\partial \gamma_U}{\partial T}\right)_{A, N_i^*, \epsilon_{ij}^{\parallel}, \sigma_{ij}^{\perp}} = T \left(\frac{\partial \gamma_S}{\partial T}\right)_{A, N_i^*, \epsilon_{ij}^{\parallel}, \sigma_{ij}^{\perp}}. \quad (25)$$

The calculation of  $\gamma$  and  $\gamma_U$  as a function of temperature has frequently revealed a slight curvature.<sup>27</sup> This enables the adjustment

of  $\gamma_U$  through a second-order polynomial expansion, omitting the linear term to allow  $\gamma_S = 0$  at  $T = 0$  K for the determination of the integration constant. The method based on fitting using simple polynomial functions is empirical because the fitting parameters may not have physical meaning,

$$\begin{aligned} \gamma_U &= A + CT^2 \rightarrow \frac{\partial \gamma_S}{\partial T} = 2C \rightarrow \gamma_S \\ &= 2CT + K \rightarrow \gamma_S = 2CT \rightarrow \gamma_F = A - CT^2, \end{aligned} \quad (26)$$

where K is an integration constant, determined considering that  $\gamma_S$  is zero at  $T = 0$  K. In Fig. 2, I present the experimental surface free energy of water in the liquid–vapor phase [Fig. 2(a)] and the SFE of aluminum in the solid–liquid phase [Fig. 2(b)], along with their respective fittings using a linear function and a second-order polynomial without a linear term. As depicted in Figs. 2(a) and 2(b), the polynomial fit proves to be better suited for adjusting the SFE. Let me note that the Surface Interface Energy (SIE) could also be approximated using other types of functions, subject to the following constraints: (i) at  $T = 0$  K, the entropy must be zero, implying that the fitting function for  $\gamma_U$  must be defined in such a way that the integration of its derivative with respect to T, divided by T ( $\gamma_S$ ), is well-defined at  $T = 0$  K, and (ii)  $\gamma_S$  must be positive, similar to  $\gamma_U$  and  $\gamma_F$ , and should be an increasing function. Classical thermodynamics does not provide an exact relationship for the temperature dependence of the internal energy of liquids. For the majority of isotropic liquids, this internal energy is a monotonically increasing convex function concerning temperature. Polynomials are most commonly used for smoothing experimental data obtained for a single set of measurements and for correlating large sets of data.

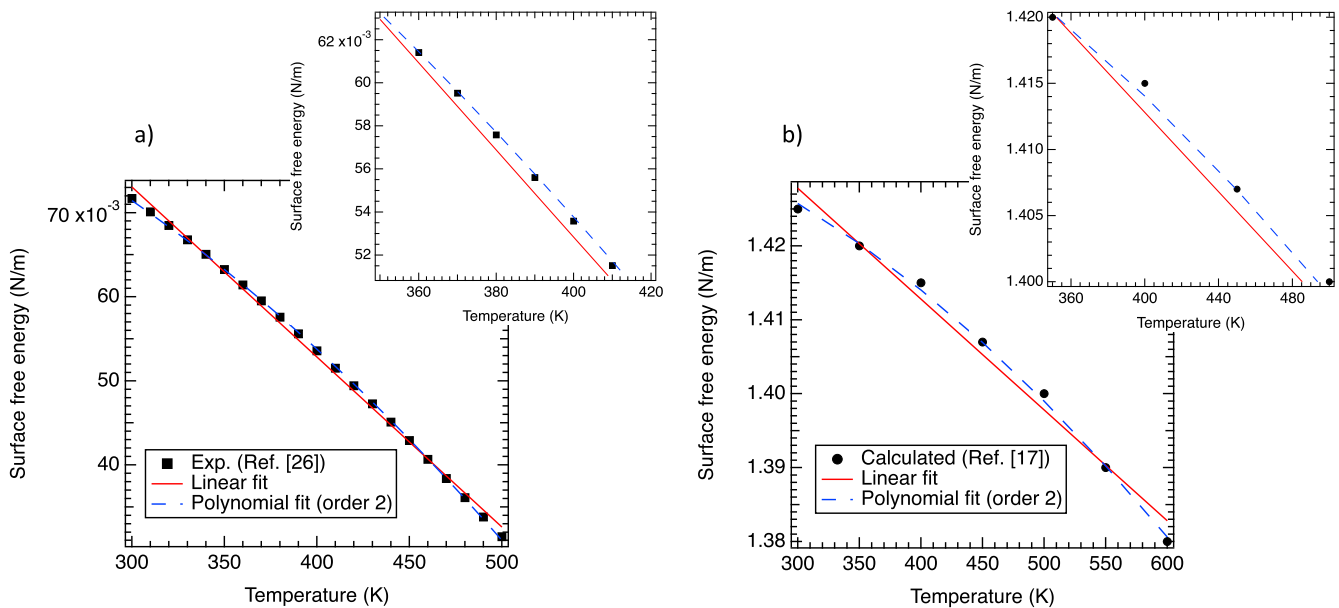


**FIG. 2.** The experimental surface free energy of the water liquid–vapor interface<sup>28</sup> (a) and the calculated surface free energy of copper solid–liquid<sup>27</sup> (b) along with their respective adjustments using both linear and second-order polynomial models (without a linear term).

Thermodynamically, it is well known that the heat capacity can be defined as a polynomial of order  $n$  such as  $c_v = \sum_{i=0}^n C_i T^i$ , where  $C_i$  are constants and  $T$  is the temperature. Since  $c_v = \frac{\partial U}{\partial T}$ , where  $U$  can be defined, after integration, as  $U = K + \sum_{i=0}^n \frac{C_i}{i+1} T^{i+1}$ , with  $K$  a constant, I can derive  $\gamma_U = \frac{U}{S} = \frac{K + \sum_{i=0}^n \frac{C_i}{i+1} T^{i+1}}{S}$ . Interestingly,  $\gamma_U$  could also be evaluated from statistical physics as  $\gamma_U = \frac{U}{S} = \frac{k_B T}{SQ} \frac{\partial Q}{\partial T} = \left[ \left\langle \frac{U}{S} \right\rangle - \frac{T}{S} \left\langle \frac{\partial U}{\partial T} \right\rangle \right]$ . As  $U$  can be defined from a thermal polynomial of order  $n$ ,  $\gamma_U$  can thus also be described in this way.

Below, I sum up the main equations involving the operational expression allowing the calculation of  $\gamma_F$  from Eq. 26:

- Equation (11),  $\gamma = \gamma_F - \sum_i \mu_i \Gamma_i^*$  such as  $\Gamma_i^* = \frac{N_i^*}{A}$ .
- Equation (12),  $\gamma = \gamma_F + A \left( \frac{\partial \gamma_F}{\partial A} \right)_{T, N_i^*, \epsilon_{ij}^{\parallel}, \sigma_{ij}^{\perp}}$ .
- Equation (14),  $\gamma_S = - \left( \frac{\partial \gamma_F}{\partial T} \right)_{A, N_i^*, \epsilon_{ij}^{\parallel}, \sigma_{ij}^{\perp}}$ .
- Equation (17),  $d\gamma_F = -\gamma_S dT + \sum_i d\Gamma_i \mu_i + \sum_{ij} \left[ \delta \epsilon_{ij}^{\parallel} (\tau_{ij} - \gamma \delta_{ij}) + \sigma_{ij}^{\perp} \delta_{ij} \right]$ .
- Equation (18),  $\gamma_S = - \left( \frac{\partial \gamma}{\partial T} \right)_{\mu_i, \epsilon_{ij}^{\parallel}, \sigma_{ij}^{\perp}} = - \left( \frac{\partial \gamma_F}{\partial T} \right)_{N_i, \epsilon_{ij}^{\parallel}, \sigma_{ij}^{\perp}}$ .
- Equation (25),  $\left( \frac{\partial \gamma_U}{\partial T} \right)_{A, N_i^*, \epsilon_{ij}^{\parallel}, \sigma_{ij}^{\perp}} = T \left( \frac{\partial \gamma_S}{\partial T} \right)_{A, N_i^*, \epsilon_{ij}^{\parallel}, \sigma_{ij}^{\perp}}$ .

### C. When the solid is rigid

The calculation of  $\gamma$  can thus be directly performed from Eq. (9), which is written as

$$dF^* = -S^* dT + \gamma dA + \sum_i \mu_i dN_i^* \text{ with } \gamma = \left( \frac{\partial F^*}{\partial A} \right)_{T, N_i^*}. \quad (27)$$

As the free energy of both the liquid and solid bulk phases remains unaffected by modifications in surface area (except for size effects<sup>29</sup>), I obtain

$$\gamma = \left( \frac{\partial F^*}{\partial A} \right)_{T, N_i^*} = \left( \frac{\partial F}{\partial A} \right)_{T, N_i^*} = \left\langle \frac{\partial U}{\partial A} \right\rangle_{T, N_i^*}. \quad (28)$$

Therefore,  $\gamma$  can be evaluated by perturbing the surface area using the non-exponential test area methodology (TA2<sup>7</sup>), while  $\gamma_F$  is calculated from  $\gamma_U$ . Interestingly,  $\gamma$  is always positive, while  $\gamma_U$  and  $\gamma_F$  can be negative. These negative values can be compensated by  $\sum_i \mu_i \Gamma_i$  to obtain a positive  $\gamma$ .

## III. COMPUTATIONAL DETAILS

### A. Molecular dynamics simulations

Four systems were investigated: (i) water liquid–vapor, (ii) aluminum solid–vapor, (iii) aluminum solid–water, and (iv) water–graphene interfaces. Water was modeled using the rigid TIP4P/2005 model, known for its accurate reproduction of thermodynamic and interfacial properties.<sup>30</sup> Aluminum solid was modeled using a full Lennard-Jones (LJ) potential,<sup>18</sup> which has demonstrated exceptional accuracy in predicting both mechanical and interfacial properties.<sup>17,18</sup> Graphene was treated as rigid and modeled using a pure Lennard-Jones potential.<sup>31</sup> The partial charges and Lennard-Jones parameters are provided in Table I. Interactions between water/aluminum and water/graphene were described by the LJ potential using the Lorentz Berthelot mixing rule.<sup>32,33</sup> All computed interactions were truncated at a cutoff of 12 Å. Electrostatic interactions (water/water) were handled through the Ewald sum<sup>34</sup> with a relative error of  $10^{-6}$  and a convergence parameter of  $0.29 \text{ \AA}^{-1}$ .

**TABLE I.** Lennard-Jones parameters and partial charges of different atoms of water, aluminum, and graphene. The TIP4P/2005<sup>30</sup> water model was constructed from an oxygen atom (OW), two hydrogen atoms (HW), and a fictive massless particle (MW). Geometrical characteristics of water and graphene are also provided.

Type	$\sigma$ (nm)	$\epsilon$ (kJ mol <sup>-1</sup> )	q (e)
Water			
OW	0.315 89	0.775 11	0
HW	0	0	0.5564
MW	0	0	-1.1128
Distance of OW–HW and MW–OW (nm)	0.095 72	0.015 46	
Angle of HW–OW–HM (°)	$\theta = 104.52$		
Angle of HW–OW–MM (°)	$\theta = 52.26$		
Aluminum			
Al	0.260 59	16.83	0
Graphene			
Distance Cg–Cg (nm)	0.14		
Cg	0.339 97	0.359 405 6	0

**TABLE II.** Number of molecules/atoms and final box lengths (nm) as a function of the type of interface. SV and LV correspond to the solid–vapor and liquid–vapor interfaces, respectively. For the graphene–water interface,  $L_x \neq L_y$ .

Type of interface	N	$L_x = L_y$	$L_z$
Water LV	1807	3.055	25.0
Aluminum SV	7040	3.2365	22.1638
Water–graphene	3200-416	3.1929-3.4032	9.1271
Water–aluminum	400-7040	3.2365	22.0600

**TABLE III.** Gibbs dividing surface position ( $z_G$ ) and interface thickness ( $\delta$ ) as functions of temperature were obtained from both the hyperbolic (tanh) and error (erf) functions.

Temperature (K)	$z_G$ (nm)	$\delta$ (nm)
	<b>tanh</b>	
300	3.014	0.280
320	3.038	0.305
370	3.131	0.377
450	3.209	0.427
500	3.383	0.522
	<b>erf</b>	
300	3.014	0.280
320	3.038	0.305
370	3.131	0.377
450	3.209	0.427
500	3.383	0.522

The simulations of the liquid–vapor (LV) interface were conducted in the NVT statistical ensemble, employing the Nose–Hoover algorithm<sup>35</sup> with a thermostat relaxation time of 0.1 ps. For the solid–liquid (SL) interface, the simulations were carried out in the  $Np_NAT$  statistical ensemble, utilizing the Martyna–Tuckerman–Klein Barostat,<sup>36</sup> where  $N$  represents the number of molecules,  $V$  is the volume,  $T$  is the temperature,  $p_N$  corresponds to the normal pressure at the interface, and  $A$  is the surface area. The thermostat and barostat relaxation times were set to 0.1 and 0.5 ps, respectively. The normal component of the pressure tensor,  $p_N$ , was maintained at 0.1 MPa. The integration timestep was set to 1 fs. Additionally, water dynamics were modeled using the quaternion algorithm.<sup>37</sup> All simulations were performed using the DLPOLY code.<sup>38</sup> The temperatures considered ranged from 300 to 500 K.

The equilibrium configurations of the homogeneous phases (liquid and solid phases) were obtained from 10 ns of simulations (2 ns in NVT, followed by 8 ns in  $Np_NAT$ ). The resulting configurations were then altered by elongating the  $L_z$  dimension from a liquid bulk configuration. These resulting configurations served as the initial configurations for the LV and SV MD simulations. The equilibration phase consisted of 10 ns steps, and the calculation of the average properties was carried out over an additional 20 ns during the acquisition phase. Aluminum–water and graphene–water simulations were conducted by equilibrating a central aluminum box surrounded by two water boxes for 2 ns in NVT, followed by 10 ns in  $Np_NAT$ , and 20 ns for the acquisition phase. The initial configuration of aluminum corresponds to the crystallographic structure,<sup>18</sup> a cubic face-centered structure in which the interface lies along the plane 0,0,1, while water molecules were randomly inserted.

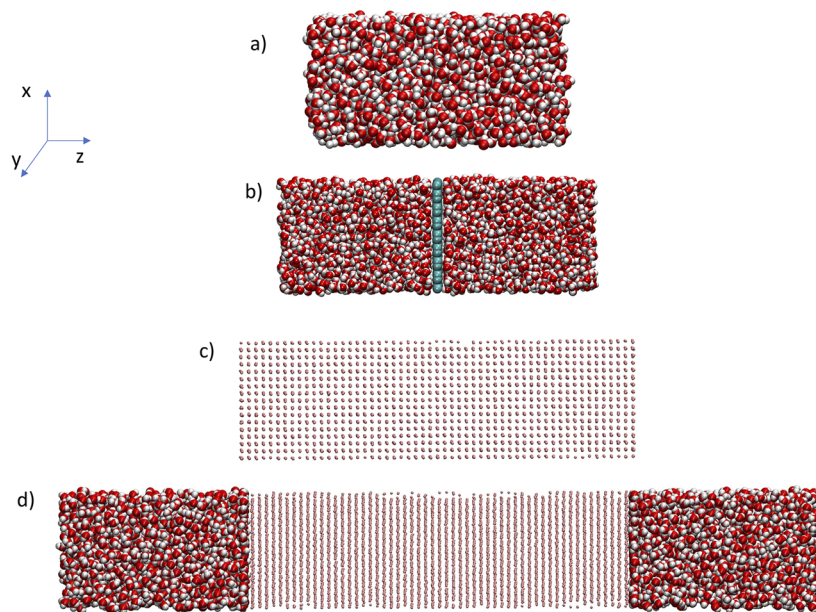


**FIG. 3.** Snapshots of each studied system: (a) Water Liquid–Vapor (LV), (b) water–graphene, (c) aluminum Solid–Vapor (SV), and (d) water–aluminum interfaces.

The number of molecules and the final length of the simulation box are provided in Table II. Illustrations of each system are also provided in Fig. 2. Input and output files are freely accessible through the GitHub server files.

## IV. RESULTS

### A. Water liquid-vapor interface

As shown in Fig. 1(b), the calculation of Surface Internal Energy (SIE) requires the determination of both liquid ( $L_-^l$  and  $L_+^l$ ) and vapor ( $L_-^v$  and  $L_+^v$ ) phases. To achieve this, density profiles along the  $z$  direction were calculated from the center of mass of water molecules at each temperature and fitted with a hyperbolic tangent function<sup>39-41</sup> based on mean-field theory<sup>42,43</sup> [ $\rho(z) = 0.5(\rho_l + \rho_v) - 0.5(\rho_l - \rho_v)\tanh(2(z - z_G)/\delta)$ ], where  $\rho_l$ ,  $\rho_v$ ,  $z_G$ , and  $\delta$  represent the liquid density, vapor density, position of the Gibbs dividing surface, and the thickness of the interface, respectively. The center of mass of the simulation box was located at the origin (0,0,0). Figure 4(a) displays the density profiles at  $T = 300$  K and  $T = 450$  K, along with their respective fits using the hyperbolic tangent function. As depicted in Fig. 4(a), the profiles are flat, indicating that the system is well-sampled, and the hyperbolic function appears to be well-suited for fitting the density profiles. Furthermore, the temperature effect is accurately reproduced, demonstrating good agreement with the experiment [Fig. 4(a)]. The liquid and vapor phases were selected such that  $L_{-/+}^l = -/+ + z_G + / - \delta$  and  $L_{-/+}^v = z_G - / + \delta$ . All parameters from 300 to 450 K are reported in Table III.

In the case of a planar liquid-vapor (LV) interface with one component,  $\gamma = \gamma_F = \tau$  with  $\tau = \tau_{xx} = \tau_{yy}$ , the stress tension in the  $x$  and  $y$  directions is identical because  $L_x = L_y$  (where  $L$  is the box length). Surface internal energy was calculated and is presented as a function of temperature ( $T$ ) in Fig. 4(b). At 300 K,  $\gamma_U = 113.7$  mN/m (including the long-range contribution calculated from the corrected energy<sup>44</sup>). As shown in this figure, SIE increases with increasing  $T$ , suggesting that the interfacial region becomes more cohesive as  $T$  rises, counterbalancing the thermal effect and the associated increase in disorder. Figure 4(b) illustrates that, in contrast to  $\gamma_U$ ,  $\gamma$  (calculated using the non-exponential test-area method, TA2<sup>7</sup>) decreases with increasing  $T$  because the entropic contribution is well accounted for and consistent with experimental data.<sup>28</sup> Additionally,  $\gamma$  was evaluated from an adjustment of  $\gamma_U$  using Eq. (26) with the following adjusted parameters:  $A = 87.0751$  mN/m and  $C = 0.00017286$  mN/m/K<sup>-2</sup>. Figure 3(b) demonstrates that the function used in Eq. (26) is well-suited for adjusting  $\gamma_U$ . Furthermore, Fig. 4(b) highlights that  $\gamma$  calculated through this method aligns well with surface free energy obtained from TA2. The increase of  $\gamma_U$  with  $T$  corresponds to the increase in the interfacial energy due to the enlargement of the interface thickness ( $\delta$ ), which increases by a factor of 2 from 300 to 500 K (Table III).

Fitting the density profile only concerns the liquid-vapor interface since both phases are not clearly defined, unlike the solid-liquid interface. To assess the dependence of the Surface Free Energy (SFE) and Surface Interface Energy (SIE) on the fitting function, I tested an

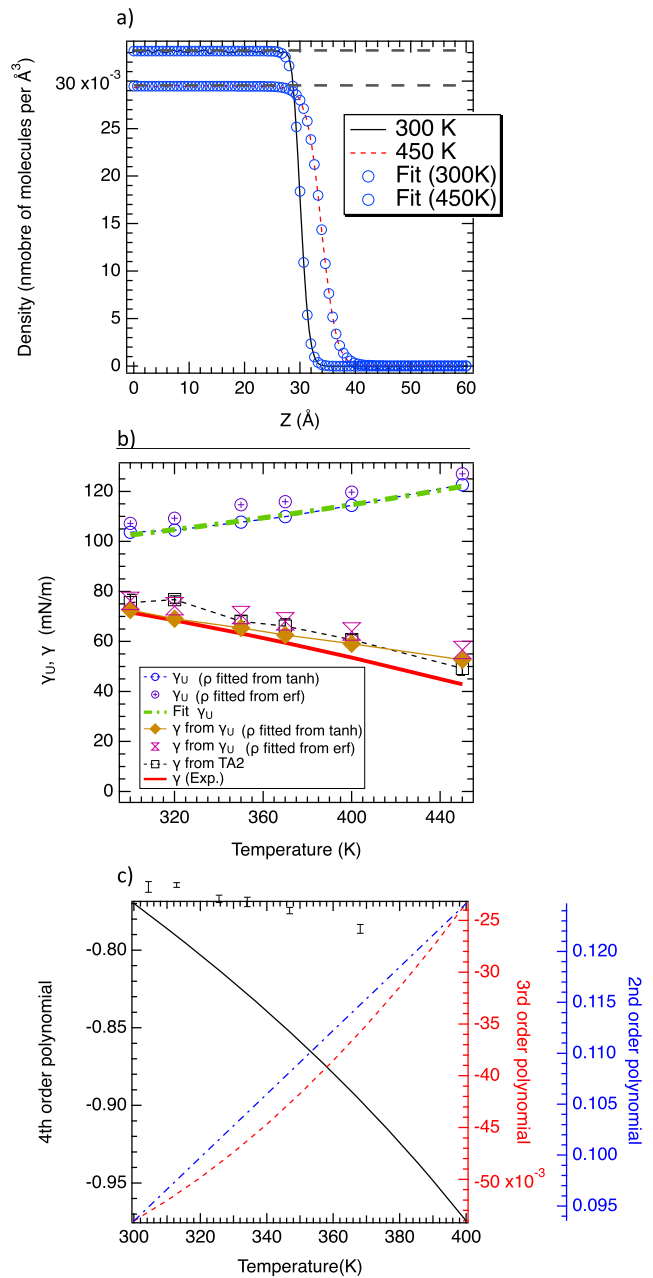


**FIG. 4.** (a) Density profile of the center of mass of water molecules at the liquid-vapor interface at 300 and 450 K. The profiles are shown between 0 and 60 Å due to the symmetry of the planar system. Horizontal dashed gray lines correspond to the experimental data.<sup>28</sup> (b) Surface free energy and surface internal energy of the water liquid-vapor interface as functions of temperature. Error bars are not shown due to their insignificance; the average values obtained were  $\Delta\gamma = 2.9$  mN/m and  $\Delta\gamma_U = 3.2$  mN/m. (c) Surface entropy of the water liquid-vapor interface is represented using second, third, and fourth order polynomials.

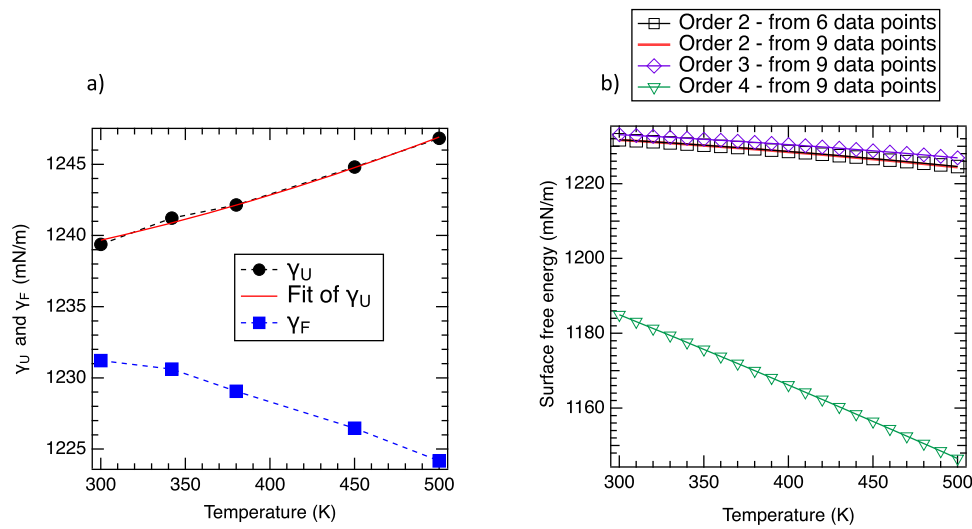


**FIG. 5.** (a) Surface free energy and surface internal energy of the water–aluminum solid–vapor interface as a function of temperature. (b) Calculated surface free energy using various fitting equations.

error function (erf) associated with capillary wave<sup>45</sup> theory to adjust the liquid–vapor density profile. Interface thickness and Gibbs positions are reported in Table III, while SFE and SIE are plotted in Fig. 4(a). As highlighted in this figure, the final SFE and SIE are weakly impacted by the fitting function. It is worth mentioning that the solid–liquid (SL), liquid–liquid (LL), and solid–vapor (SV) interfaces do not need to precisely define the position of the interface because both phases are clearly defined, unlike the liquid–vapor (LV) interface. Additionally, I tested polynomials of orders 2, 3, and 4, excluding the linear term to align with the requirement that  $\gamma_s$  must be positive and an increasing function. Figure 4(c) depicts the evolution of surface entropy as a function of temperature. As illustrated in this figure, only the quadratic polynomial satisfies these constraints. For polynomials of order  $n$  higher than 2,  $\gamma_s$  was calculated from the integration of the derivative of  $\gamma_U$  with respect to  $T$ , as in Eq. (26),  $\gamma_U = A + \sum_{i=2}^n C_i T^i$ ,  $1/T d\gamma_U/dT = \sum_{i=2}^n i C_i T^{i-2}$ , and  $\gamma_s = \sum_{i=2}^n (i/(i-2)) C_i T^{i-1}$ . In this case, this justification supports the utilization of a second-order polynomial to fit  $\gamma_U$ . The polynomials of higher orders ( $>2$ ) did not satisfy the aforementioned

constraints due to the limited number of data points (5 temperatures). This point will be discussed in this section.

### B. Aluminum solid–vapor interface

I present in Fig. 5(a) the surface free energy and surface internal energy as functions of temperature. Let us mention that, as

**TABLE V.** Fit coefficient values and their error deviations,  $a_0$  (mN/m),  $a_1$  (mN/m/K),  $a_2$  (mN/m/K<sup>2</sup>), and  $a_3$  (mN/m/K<sup>2</sup>).

Coefficients	Value	Error bars
a0	$a_0 + a_1 T^2$ ; 6 temperatures	
	1235.8	0.504
a1	$4.4822 \times 10^{-5}$	$2.98 \times 10^{-6}$
a0	$a_0 + a_1 T^2$ ; 9 temperatures	
	1235.7	0.422
a1	$4.5528 \times 10^{-5}$	$2.64 \times 10^{-6}$
a0	$a_0 + a_1 T^2 + a_2 T^3$ , 6 temperatures	
	1232.8	1.45
	$1.0272 \times 10^{-4}$	$2.74 \times 10^{-5}$
a2	$-8.4105 \times 10^{-8}$	$4.44 \times 10^{-8}$
a0	$a_0 + a_1 T^2 + a_2 T^3$ , 9 temperatures	
	1232.4	1.3
	$1.105 \times 10^{-4}$	$2.47 \times 10^{-5}$
a2	$-1.0655 \times 10^{-7}$	$4.04 \times 10^{-8}$
a0	$a_0 + a_1 T^2 + a_2 T^3 + a_3 T^4$	
	1219.9	5.38
	$6.0766 \times 10^{-4}$	$2.11 \times 10^{-4}$
	$-1.771 \times 10^{-6}$	$7.07 \times 10^{-7}$
a3	$1.5428 \times 10^{-9}$	$6.53 \times 10^{-10}$

**TABLE IV.** SFE and stress tension of the aluminum solid–vapor system as functions of temperature. For SFE and stress tension, the average standard deviation is 3.5 and 2.9 mN/m, respectively.

Temperature (K)	$\gamma_F$ (mN/m)	$\tau$ (mN/m)
300	1231.22	147.01
342	1230.62	104.11
370	1229.06	98.65
450	1226.46	82.19
500	1224.17	64.79

shown in Eq. (11) in the case of the solid–vapor interface,  $\gamma = \gamma_F$ , and then they can be used interchangeably. SFE was calculated through an adjustment of SIE. As shown in Fig. 5(a), SIE exhibits a temperature dependence similar to that of the water liquid–vapor interface, namely an increase with increasing T. The decrease in SFE with increasing T is well captured, indicating that both the thermal effect and the associated entropic contribution are appropriately accounted for in our calculation. At 300 K, I obtain a surface tension of 1231 mN/m, in line with experimental data, which reported values of 1218 mN/m for the {111} surface<sup>18</sup> and 1160 mN/m from the cleaving method.<sup>17</sup> Notably, the surface entropy can be directly calculated by averaging  $\gamma_S = (\gamma_U - \gamma_F)/T$  from 300 to 500 K, and this result can be compared with the relation  $\gamma_S = -\frac{\partial \gamma_F}{\partial T}$ . I obtain a similar result of 0.035 743 mN/m/K through direct averaging and 0.036 244 mN/m/K from a linear fit of  $\gamma_F$ . Additionally, I provide the stress tension  $\tau$  as a function of T. As indicated in Table IV, both the stress tension and surface tension decrease as T increases, in contrast to  $\gamma_U$ , suggesting that an entropic term is also involved in  $\tau$ .

The accuracy of the fitting procedure is correlated with the number of data points available. For a limited dataset (typically

**TABLE VI.**  $\gamma_U$  and its various contributions (mN/m) as a function of temperature (K) for the graphene–water interface. Standard deviations are provided in subscripts such that  $-45.3_3 = -45.3 \pm 0.3$  mN/m.

Temperature	$\gamma_U$	$\gamma_U(\text{H}_2\text{O}/\text{H}_2\text{O})$	$\gamma_U(\text{graphene}/\text{H}_2\text{O})$
300	$-45.3_3$	62.6 <sub>9</sub>	$-127.8_4$
320	$-47.7_2$	47.1 <sub>8</sub>	$-127.8_5$
370	$-40.4_3$	50.7 <sub>5</sub>	$-118.7_6$
420	$-39.1_2$	32.9 <sub>6</sub>	$-109.4_8$
500	$-28.4_2$	14.5 <sub>5</sub>	$-93.2_6$

5–6 temperatures), employing a second-order polynomial appears appropriate, as indicated by the deviation errors on the fitted parameters (Table V). However, when employing a polynomial of a higher degree with such limited data, the error bars on the fit coefficients escalate (Table V), resulting in pronounced deviations in their derivatives and subsequently introducing spurious entropic terms. To mitigate this issue, expanding the data range becomes imperative. As depicted in Fig. 5(b), when a third-order polynomial is utilized, fair outcomes to those of the second order are achieved, while a fourth-order polynomial involves a drastic deviation of surface free energy in line with the bar errors reported in Table V.

### C. Water liquid–rigid graphene interface

The positions of the interfacial region were determined by calculating the density profile of the centers of mass of water molecules. As depicted in Fig. 6(a), molecular oscillations close to the graphene surface are observed, likely due to excluded volume effects, which extend the interface limit to about 20 Å. The surface free energy and surface internal energy were then predicted and are presented in Fig. 6(b). Similar to the liquid–vapor interfaces, SIE increases with rising temperatures. However, in this case, SIE is negative and not compensated by the entropic term, resulting in a negative  $\gamma_F$ . In contrast,  $\gamma$  calculated from TA2 and  $\tau$  [Eq. (2)] is positive and decreases as T increases. This could be attributed to (i) a positive interfacial excess amount ( $\Gamma_{\text{H}_2\text{O}}$ ) that counterbalances the negative  $\gamma_F$ , potentially allowing for the extraction of  $\Gamma_{\text{H}_2\text{O}}$  via  $\Gamma_{\text{H}_2\text{O}} = (\gamma_F - \gamma)/\mu_{\text{H}_2\text{O}}$ . The chemical potential of water according to TIP4P/2005 is  $-32$  kJ/mol<sup>6</sup>, leading to  $\Gamma_{\text{H}_2\text{O}} = 0.0287$  Å<sup>2</sup>, equivalent to about 31 water molecules per interface in the first layer; (ii) the absence of a solid contribution term in  $\gamma_U$  that could compensate for the negative contribution arising from water/water and water/graphene interactions (this point will be discussed later).

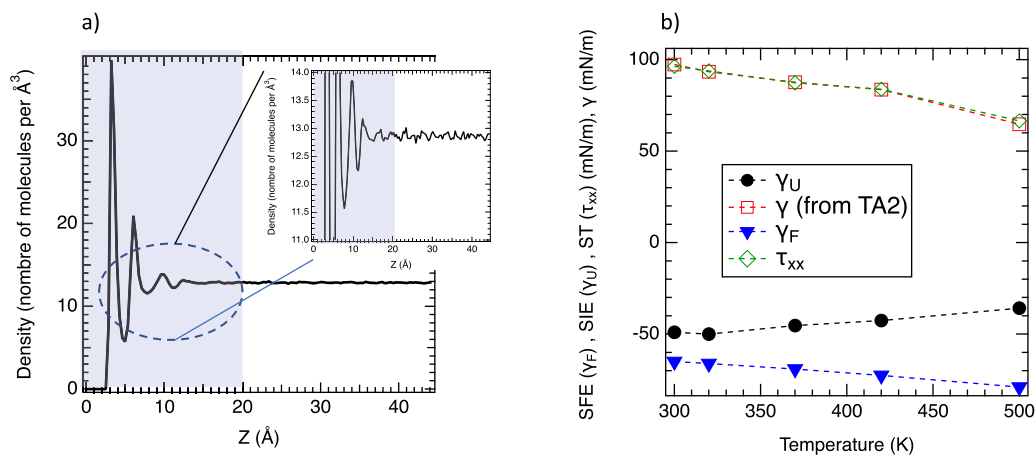


**FIG. 6.** (a) Density profile of the center of mass of water molecules at the graphene–liquid water interface at 300 K. The profiles are depicted between 0 and 50 Å due to the symmetry of the planar system. (b) Surface free energy, surface internal energy, and stress tension of the graphene–liquid water interface as a function of temperature. Error bars are omitted due to their insignificance; the average values obtained were  $\Delta\gamma = 0.9$  mN/m and  $\Delta\gamma_U = 0.5$  mN/m.

### D. Aluminum–water solid–liquid interface

Bulk liquid and solid contributions have been calculated on a slab of 10 Å to ensure they are far from the solid–liquid interfaces. In Fig. 7(a), I present  $\gamma_U$  and  $\gamma_F$  as functions of temperature. This figure illustrates that  $\gamma_U$  is well-fitted by the commonly used second-order polynomial [Eq. (26)], showing an increase with temperature. On the other hand,  $\gamma_F$  decreases as the temperature rises. These results align with observations made for the liquid–vapor, solid–vapor, and graphene–water interfaces. Interestingly, the obtained  $\gamma_U$  and  $\gamma_F$  are weaker than those calculated for the solid–vapor interface (Fig. 5). To further understand these contributions, I evaluated different components of  $\gamma_U$ , namely  $\gamma_U^{Al/Al}$ ,  $\gamma_U^{H_2O/H_2O}$ , and  $\gamma_U^{Al/H_2O}$ . As shown in Fig. 7(b),  $\gamma_U^{Al/Al}$  is of similar magnitude to

$\gamma_U^{SV}$  of the Al–vapor interface reported in Fig. 5, and it follows a similar trend with temperature. Unlike  $\gamma_U^{Al/Al}$ , both  $\gamma_U^{H_2O/H_2O}$  and  $\gamma_U^{Al/H_2O}$  are negative, indicating a tendency to “create” surface. The negative contribution [ $\gamma_U^{H_2O/H_2O} + \gamma_U^{Al/H_2O}$ ] is then compensated by the positive  $\gamma_U^{Al/Al}$ . In the case of the graphene–water interface,  $\gamma_U$  is also found to be negative [Fig. 6(b)] and is not compensated due to the rigidity of graphene (Table VI). Furthermore, in both solid–water interfaces,  $\gamma_U^{(solid/H_2O)} < 0$  and  $\gamma_U^{(solid/H_2O)} < \gamma_U^{H_2O/H_2O}$ , indicating a strong wetting tendency.

These results seem to suggest that considering the material rigid may not be suitable for evaluating interfacial properties. This observation holds true in all cases except for  $\gamma$  of the graphene–water interface, which is of the right order of magnitude in comparison

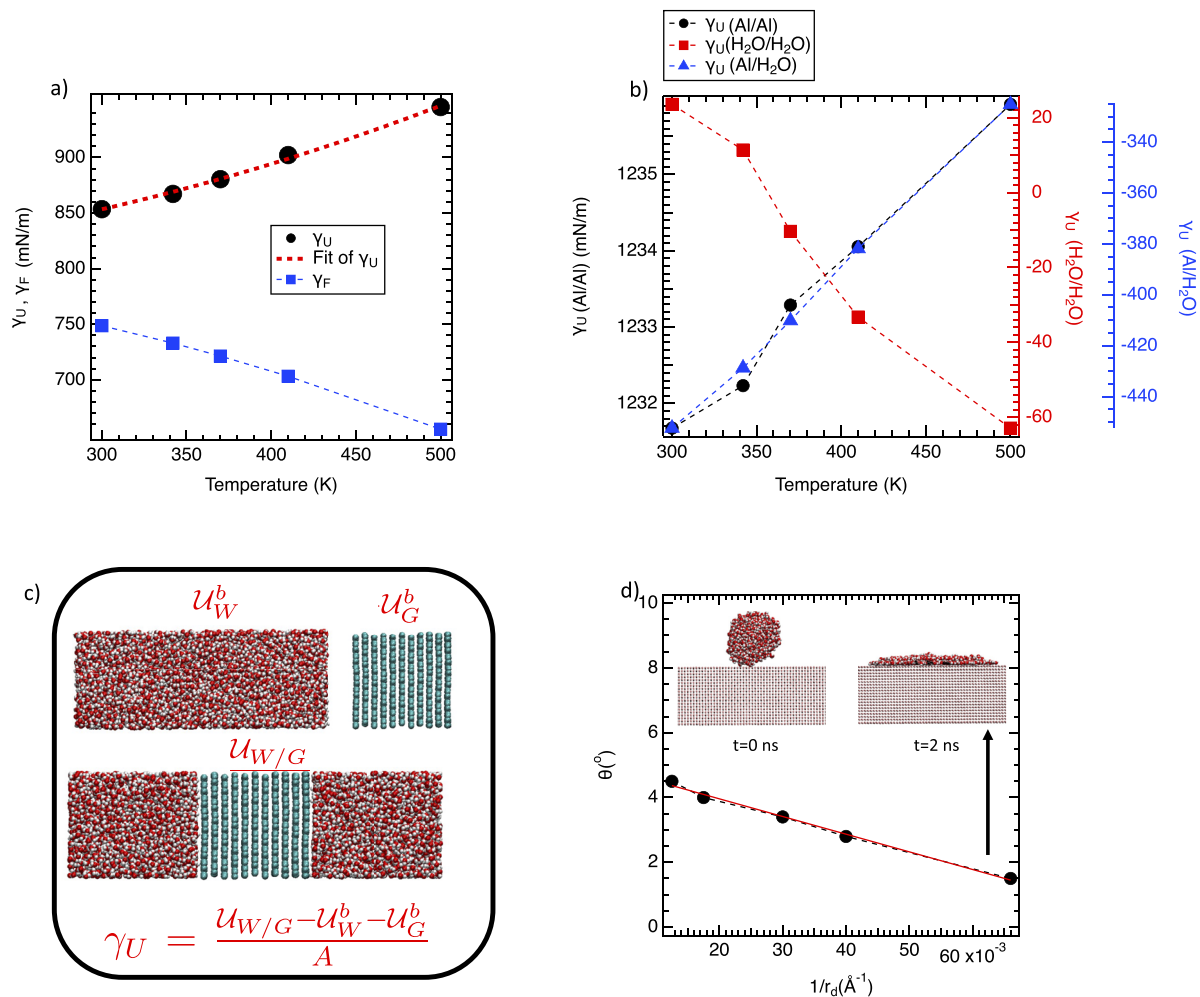


**FIG. 7.** (a) Surface free energy and surface internal energy of the aluminum–water interface as a function of temperature. Error bars are omitted due to the small values; the average obtained was  $\Delta\gamma = 12.5$  mN/m and  $\Delta\gamma_U = 12.8$  mN/m. (b) Contributions of  $\gamma_U^{Al}$  (black circle and left axis),  $\gamma_U^{H_2O}$  (red square and right axis), and  $\gamma_U^{Al-H_2O}$  (blue triangle and right axis) as a function of temperature. (c) Illustration of different configurations for calculating water-multilayer graphene surface tension. (d) Contact angles on aluminum surfaces as a function of droplet radius ( $r_d$ ) at 300 K.

**TABLE VII.**  $\gamma_U$  and its various contributions (mN/m) for the aluminum–water solid–liquid interface at 300 K for both flexible and rigid surfaces. Standard deviations are provided in subscripts such that  $1231.1_{12} = 1231.1 \pm 12$  mN/m.

Type	$\gamma_U$	$\gamma_U(\text{H}_2\text{O}/\text{H}_2\text{O})$	$\gamma_U(\text{Al}/\text{H}_2\text{O})$	$\gamma_U(\text{Al}/\text{Al})$
Rigid	-426.6 <sub>5</sub>	29.8 <sub>2</sub>	-451.4 <sub>9</sub>	
Flexible	852.3 <sub>9</sub>	30.2 <sub>3</sub>	-452.2 <sub>8</sub>	1231.1 <sub>12</sub>

**TABLE VIII.**  $\gamma_U$  (mN/m) for multiple layer graphene–water interface at 300 K for both flexible and rigid surfaces.

	$\mathcal{U}_{W/G} (\times 10^5)$	$\mathcal{U}_W^b (\times 10^5)$	$\mathcal{U}_G^b (\times 10^4)$	$\gamma_U$
Rigid	-1.532	-1.527	...	-37.2
Flexible	-1.238	-1.527	2.57	238.1

with the liquid–vapor interface. Therefore, the  $\gamma$  calculated for the rigid form, which corresponds to  $\gamma(\text{H}_2\text{O}/\text{H}_2\text{O}) + \gamma(\text{Graphene}/\text{H}_2\text{O})$ , offers only a partial representation and cannot be equated to  $\gamma$ . To further emphasize this point, I prepared a rigid block of Al that I brought into contact with two water reservoirs. The resulting  $\gamma_U$  and its various contributions at 300 K are reported in Table VII. As shown in this table, the rigid solid exhibits a negative  $\gamma_U$ , contrary to the flexible block. This negative value arises from  $\gamma_U(\text{Al}/\text{H}_2\text{O})$ , which remains similar in both rigid and flexible cases, as well as  $\gamma_U(\text{H}_2\text{O}/\text{H}_2\text{O})$ . These findings underscore the significance of the solid contribution [ $\gamma_U(\text{Al}/\text{Al})$ ], which counterbalances the negative  $\gamma_U(\text{Al}/\text{H}_2\text{O})$ .

If I explicitly consider the water/flexible-monolayer graphene interface, using Eq. (20) to calculate  $\gamma_U$  is not feasible because the energy of a graphene monolayer in the bulk phase is not computable (due to the impossibility of defining a pure graphene bulk phase without a graphene/vapor interface). To address this issue, I decided to model the interfacial system (W/G), the water (W), and a multi-layer graphene (G) bulk phase separately, with similar simulation box sizes and molecule numbers [see Fig. 7(c)]. I chose a multi-layer graphene with 11 monolayers to ensure a sufficiently large bulk graphene phase, allowing the use of a cutoff of 12 Å and the NpnAT statistical ensemble. Under these conditions, Eq. (20) becomes  $\gamma_U = \frac{\mathcal{U}_{W/G} - \mathcal{U}_W^b - \mathcal{U}_G^b}{A}$ . The flexibility of graphene was modeled by considering intramolecular potentials (torsion, bending, and bonding).<sup>46,47</sup> The energy of each phase and the Surface Interface Energy (SIE) are provided in Table VIII. This table reveals a drastic difference between rigid and flexible graphene, as a negative value of  $\gamma_U$  is found for the rigid case, aligning with the results obtained from monolayer graphene and rigid aluminum. On the contrary, a positive value is obtained from the flexible structure, confirming our previous assertion about the strong impact of the solid contribution.

To offer further validation of the developed methodology, I evaluated  $\gamma^{SL}$  of the aluminum–water interface from  $\gamma_F^{SL}$  by combining Eq. (11) ( $\gamma^{SL} = \gamma_F^{SL} - \sum_i \mu_i \Gamma_i^*$ ) and the Young's equation

( $\gamma^{SL} - \gamma^{SV} + \gamma^{LV} \cos \Theta = 0$ ), where  $\Theta$  is the Young's angle. Indeed, by extracting  $\sum_i \mu_i \Gamma_i^*$  and calculating  $\Theta$ , I obtain

$$\sum_i \mu_i \Gamma_i^* = \gamma_F^{SL} - \gamma^{SL} = \gamma_F^{SL} - \gamma^{SV} + \gamma^{LV} \cos \Theta. \quad (29)$$

By evaluating  $\sum_i \mu_i \Gamma_i^*$  and  $\gamma_F^{SL}$ , I obtain  $\gamma^{SL}$  from

$$\gamma^{SL} = \gamma_F^{SL} - \sum_i \mu_i \Gamma_i^* = \gamma^{SV} - \gamma^{LV} \cos \Theta. \quad (30)$$

The subscript 1 corresponds to the route utilizing  $\gamma_F$  and  $\Theta$ .  $\Theta$  was determined by modeling various water nanodroplets, distinguished by the droplet's radius ( $r_d$ ), deposited on an aluminum surface. The calculation of  $\Theta$  was performed using the method developed by Essafri *et al.*<sup>48</sup> Four equilibrated droplets ( $r_d = 57, 33, 25, 15$  Å) deposited on an equilibrated aluminum surface, ranging from 25 to 50 nm over 6 nm in thickness, were considered. Through a linear fit [Fig. 7(d)], I determined that  $\Theta = 5.5^\circ$ , which is in good agreement with the experimental value<sup>49</sup> of  $\Theta = 4.6^\circ$ . The illustration of the water nanodroplet provided in Fig. 7(d) highlights the strong wettability of water over the aluminum surface.

From the values of  $\Theta$  and  $\gamma^{LV}$ , I found  $\gamma_1^{SL} = 1160$  mN/m and  $\sum_i \mu_i \Gamma_i^* = -472.5$  mN/m. In a second step, I evaluated  $\gamma^{SL}$  using the phantom wall method<sup>14</sup> ( $\gamma_2^{SL}$ ), wherein the water/aluminum interactions were progressively switched off through the free energy perturbation method.<sup>50</sup> The corresponding free energy difference was then evaluated such that

$$\gamma_2^{SL} = \gamma^{LV} + \gamma^{SV} - \frac{\Delta F}{S}. \quad (31)$$

Subscript 2 corresponds to the route using the phantom wall method.  $\Delta F$  is calculated following the method developed by Leroy and Müller-Plathe,<sup>14</sup> where the perturbation of water/aluminum interactions occurs through the coupling parameter  $\lambda$ . This is expressed as  $\epsilon_{W/Al}(\lambda) = \lambda \epsilon_{W/Al}^1 + (1 - \lambda) \epsilon_{W/Al}^0$ . Here,  $\epsilon_{W/Al}$  represents the energetic parameter of the Lennard-Jones potential, given by  $\epsilon_{W/Al} = \sqrt{\epsilon_{Al/Al} \epsilon_{W/W}}$ . The parameter  $\lambda$  varies from 0 to 1 in ten windows ( $N_w$ ).  $\frac{\Delta F}{S}$  represents the work of adhesion of water to aluminum, and it is defined as  $\Delta F = \sum_\lambda \Delta F_\lambda = -k_B T \ln(\exp(-\Delta U(\lambda)))$ , where  $U(\lambda)$  is the difference in configurational energy corresponding to the LJ potential, given by  $U(\lambda) = U(\lambda - 1) - U(\lambda)$  and  $\lambda = 1/N_w$ . Through this approach, I determined a work of adhesion of 230 mN/m.  $\gamma^{SL} 2$  is then found to be 1072 mN/m, in fair agreement with  $\gamma^{SL} 1$ , serving as an indirect validation of the developed methodology.

### E. *n*-Dodecane–water liquid–liquid interface

To validate the developed methodology, I applied it to calculate the Surface Free Energy (SFE) and Surface Interface Energy (SIE) of the oil (*n*-dodecane)–water interface. The united atom TraPPE<sup>51</sup> force field was utilized to model *n*-dodecane, and the TIP4/2005<sup>50</sup> force field was used for water. The methodology closely follows that of the solid–liquid interface, with the distinction of replacing the solid phase at the center of the simulation box with *n*-dodecane (see inset of Fig. 8). Figure 8 illustrates that  $\gamma_U$  is well-fitted by the commonly used second-order polynomial, allowing for a Surface Free Energy (SFE) in good concordance with the TA2 method and

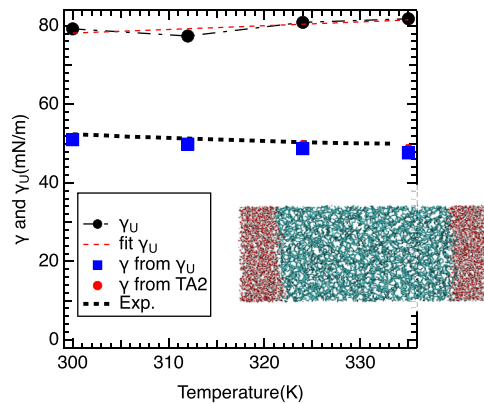


**FIG. 8.** Surface tension and surface internal energy of the *n*-dodecane–water interface as functions of temperature. A snapshot of the typical configuration at 324 K is reported in the inset.

experimental results.<sup>52</sup> These results demonstrate that, even with small amplitudes in surface tension (47–51 mN/m) and within a narrow range of temperatures (300–335 K), the developed method effectively manages Surface Free Energy (SFE).

## F. Concluding remarks

In this study, I have introduced a straightforward method to determine the surface free energy ( $\gamma_F$ ) and decouple it from the surface grand potential ( $\gamma$ ). This approach involves empirical fitting the surface internal energy ( $\gamma_U$ ) with a second-order polynomial without a linear term. By utilizing the first law of thermodynamics to express the relationship between  $\gamma_F$  and  $\gamma_S$ , I have rediscovered Shuttleworth's and Dong's relations, applied to  $\gamma_F$ , demonstrating its dependency on surface area and elasticity. Compared to the computationally expensive cleaving method, this approach required simulations of the system at various temperatures. Interestingly, I have demonstrated that methodologies based on surface area perturbation are unsuitable for calculating the interfacial properties of flexible solids. Furthermore, in the case of liquids, the interfacial energy remains constant even as the surface is stretched, leading to similarities between surface tension and interfacial energy. However, for solids, even with high elastic constants, these two contributions diverge due to alterations (even very small) in the atomic structure of the solid surface during elastic deformation. On the contrary, in the case of a rigid structure, surface free energy and surface tension become similar in the absence of deformation. However, I demonstrated that this situation involves unphysical negative SIE. To remedy it, it is crucial to consider the material's flexibility as weak as it is (high elastic coefficient).

The developed method has been applied to various interface types, demonstrating good agreement between the calculated surface free energies and experimental values. While this method effectively extracts  $\gamma_F$ , it is important to note that the surface grand potential ( $\gamma$ ) cannot be directly calculated. For a one-component liquid–vapor (LV) and solid–vapor (SV) interface,  $\gamma_F$  aligns with  $\gamma$  when considering the Gibbs dividing surface. In a multi-component LV system,  $\gamma$  can be determined using surface area perturbation, while the method developed in this work can be

employed to evaluate  $\gamma_F$ ,  $\gamma_U$ , and  $\gamma_S$ . For the solid–liquid interfaces,  $\gamma_F$ ,  $\gamma_U$ , and  $\gamma_S$  are determinable while calculating  $\gamma$  via surface area perturbation is not feasible. Although  $\gamma$  cannot be directly estimated,  $\gamma_F$  offers similar insights to  $\gamma$  regarding the degree of liquid wetting on the surface. Therefore, this method provides valuable insights into interface forces ( $\gamma_U$ ) and degrees of freedom ( $\gamma_S$ ). This method could easily be applied to calculate the surface free energy of curved interfaces (such as aerosols, droplets, bubbles, etc.) without being constrained by the local definition of tensor pressure or the specific nature of the surface area perturbation. It allows access to parameters like Tolman's length or line tension, enabling the evaluation of the internal  $\gamma_F$  of confined gases or liquids in nanopores such as in metal organic materials where interfacial interactions could help to improve dynamical<sup>53</sup> or adsorption<sup>54</sup> properties, among other applications.

While the calculation of  $\gamma_U$  is entirely based on physics, the determination of  $\gamma_S$  is semi-empirical. This is because the method developed relies on physical assumptions and involves integrating a polynomial function with fitting coefficients that lack physical interpretation to describe  $\gamma_U$  as a function of temperature. This is likely the main weakness of the described method. To improve it, it will be necessary to introduce a physical interpretation of the fitting coefficients and devise a new approach to extract the integration coefficient in Eq. (26) that relates to the interfacial entropy at a reference temperature. One potential improvement could involve adding more data points at low temperatures to better capture the thermodynamic behavior near  $T = 0$  K, where  $\gamma_U \sim \gamma_F$ . Alternatively, another solution could be to rewrite Eq. (26) to compute  $\gamma_S$  using numerical integration without relying on a fitting procedure.

## ACKNOWLEDGMENTS

I am grateful to the “Agence Nationale de la Recherche” (ANR) for its financial support through the project “BIOWATER” (Grant No. ANR-22-CE06-0024-01).

## AUTHOR DECLARATIONS

### Conflict of Interest

The author has no conflicts to disclose.

## Author Contributions

**Aziz Ghoufi:** Conceptualization (equal); Data curation (equal); Formal analysis (equal); Funding acquisition (equal); Investigation (equal); Methodology (equal); Project administration (equal); Resources (equal); Software (equal); Supervision (equal); Validation (equal); Visualization (equal); Writing – original draft (equal); Writing – review & editing (equal).

## DATA AVAILABILITY

The data that support the findings of this study are available from the corresponding author upon reasonable request.

## REFERENCES

- <sup>1</sup>J. W. Cahn, *Thermodynamics of Solid and Fluid Surfaces* (American Society of Metals, 1979).
- <sup>2</sup>J. Gibbs, in *The Collected Work of JW Gibbs*, edited by N. Haven (Yale University Press, 1957), Vol. 1.
- <sup>3</sup>D. Kramer and J. Weissmuller, *Surf. Sci.* **601**, 3042 (2007).
- <sup>4</sup>J. Irving and J. Kirkwood, *J. Chem. Phys.* **18**, 817 (1950).
- <sup>5</sup>G. Gloor, G. Jackson, F. Blas, and E. de Miguel, *J. Chem. Phys.* **123**, 134703 (2005).
- <sup>6</sup>A. Ghoufi, F. Goujon, V. Lachet, and P. Malfreyt, *J. Chem. Phys.* **128**, 154716 (2008).
- <sup>7</sup>A. Ghoufi and P. Malfreyt, *J. Chem. Phys.* **136**, 024104 (2012).
- <sup>8</sup>A. Ghoufi, P. Malfreyt, and D. J. Tildesley, *Chem. Soc. Rev.* **45**, 1387 (2016).
- <sup>9</sup>R. Shuttleworth, *Proc. Phys. Soc., Sect. A* **63**, 444 (1950).
- <sup>10</sup>J. Eriksson, *Surf. Sci.* **14**, 221 (1969).
- <sup>11</sup>J. Miyazaki, J. Barker, and G. Pound, *J. Chem. Phys.* **64**, 3364 (1976).
- <sup>12</sup>J. Broughton and G. Gilmer, *J. Chem. Phys.* **84**, 5759 (1986).
- <sup>13</sup>F. Leroy, D. dos Santos, and F. Müller-Plathe, *Macromol. Rapid Commun.* **30**, 864 (2009).
- <sup>14</sup>F. Leroy and F. Müller-Plathe, *Langmuir* **31**, 8335 (2015).
- <sup>15</sup>N. D. Pasquale and R. Davidchack, *J. Chem. Phys.* **153**, 154705 (2020).
- <sup>16</sup>N. Di Pasquale and R. L. Davidchack, *J. Phys. Chem. A* **126**, 2134 (2022).
- <sup>17</sup>M. Orselly, J. Devemy, A. Bouvet-Marchand, A. Dequidt, C. Loubat, and P. Malfreyt, *J. Chem. Phys.* **156**, 234705 (2022).
- <sup>18</sup>K. Kanhaiya, S. Kim, W. Im, and H. Heinz, *npj Comput. Mater.* **7**, 18 (2021).
- <sup>19</sup>R. Benjamin and J. Horbach, *J. Chem. Phys.* **141**, 044715 (2014).
- <sup>20</sup>T. Wu and A. Firoozabadi, *J. Phys. Chem. A* **125**, 5841 (2021).
- <sup>21</sup>A. Valiya Parambathu, T. J. Pinheiro dos Santos, W. G. Chapman, and D. N. Asthagiri, *J. Phys. Chem. A* **126**, 1782 (2022).
- <sup>22</sup>R. Addula and S. Punnathanam, *J. Chem. Phys.* **153**, 154504 (2020).
- <sup>23</sup>S. Yeandel, C. Freeman, and J. Harding, *J. Chem. Phys.* **157**, 084117 (2022).
- <sup>24</sup>I. Sanchez-Burgos and J. Espinosa, *Phys. Rev. Lett.* **130**, 118001 (2023).
- <sup>25</sup>O. X. Dong, *Proc. Natl. Acad. Sci. U. S. A.* **118**(3), e2019873118 (2021).
- <sup>26</sup>P. Müller and A. Saul, *Surf. Sci. Rep.* **54**, 157 (2004).
- <sup>27</sup>T. Frolov and Y. Mishin, *Phys. Rev. B* **79**, 045430 (2009).
- <sup>28</sup>E. W. Lemmon, I. H. Bell, M. L. Huber, and M. O. McLinden, "Thermophysical properties of fluid systems," in *Webbook de Chimie NIST* (National Institute of Standards and Technology, Washington, DC, 2001).
- <sup>29</sup>F. Biscay, A. Ghoufi, F. Goujon, V. Lachet, and P. Malfreyt, *J. Chem. Phys.* **130**, 184710 (2009).
- <sup>30</sup>J. L. F. Abascal and C. Vega, *J. Chem. Phys.* **123**, 234505 (2005).
- <sup>31</sup>L. Garnier, A. Szymczyk, P. Malfreyt, and A. Ghoufi, *J. Phys. Chem. Lett.* **7**, 3371 (2016).
- <sup>32</sup>H. A. Lorentz, *Ann. Phys.* **248**, 127 (1881).
- <sup>33</sup>H. A. Lorentz, *Ann. Phys.* **248**(1), 1227 (1881).
- <sup>34</sup>P. Ewald, *Ann. Phys.* **369**, 253 (1921).
- <sup>35</sup>S. Nose, *J. Chem. Phys.* **81**, 511 (1984).
- <sup>36</sup>G. Martyna, M. Tuckerman, D. Tobias, and M. Klein, *Mol. Phys.* **87**, 1117 (1996).
- <sup>37</sup>G. Morriss and D. Evans, *Comput. Phys. Commun.* **62**, 267 (1991).
- <sup>38</sup>T. R. Forester and W. Smith, *DLPOLY, CCP5 Program Library*, Daresbury Lab., U.K., 1004.
- <sup>39</sup>J. Alexandre, D. Tildesley, and G. Chapela, *J. Chem. Phys.* **102**, 4574 (1995).
- <sup>40</sup>E. M. Blokhuis, D. Bedeaux, C. D. Holcomb, and J. A. Zollweg, *Mol. Phys.* **85**, 665 (1995).
- <sup>41</sup>I.-F. W. Kuo, C. Mundy, B. Eggimann, M. Mc-Grath, J. Siepmann, B. Chen, J. Vieceli, and D. Tobias, *J. Phys. Chem. B* **110**, 3738 (2006).
- <sup>42</sup>J. D. van der Waals, *Z. Phys. Chem.* **13U**, 657 (1894).
- <sup>43</sup>J. Cahn and J. Hilliard, *J. Chem. Phys.* **28**, 258 (1958).
- <sup>44</sup>C. Ibergay, A. Ghoufi, F. Goujon, P. Ungerer, A. Boutin, B. Rousseau, and P. Malfreyt, *Phys. Rev. E* **75**, 051602 (2007).
- <sup>45</sup>F. P. Buff, R. A. Lovett, and F. H. Stillinger, *Phys. Rev. Lett.* **15**, 621 (1965).
- <sup>46</sup>S. Deshmukh, G. Kamath, and S. Sankaranarayanan, *Soft Matter* **10**, 4067 (2014).
- <sup>47</sup>H. D'Oliveira, X. Davoy, E. Arche, P. Malfreyt, and A. Ghoufi, *J. Chem. Phys.* **146**, 214112 (2017).
- <sup>48</sup>I. Essafri, J. C. Le breton, A. Saint-Jalmes, A. Soldera, A. Szymczyk, P. Malfreyt, and A. Ghoufi, *Mol. Simul.* **45**, 454 (2019).
- <sup>49</sup>D. Trevo and H. Johnson, *J. Phys. Chem.* **62**, 833 (1958).
- <sup>50</sup>A. Ghoufi and P. Malfreyt, *Mol. Phys.* **104**, 2929 (2006).
- <sup>51</sup>M. Martin and J. I. Siepmann, *J. Phys. Chem. B* **102**, 2569 (1998).
- <sup>52</sup>S. Zeppieri, J. Rodriguez, and A. L. de Ramos, *J. Chem. Eng. Data* **46**, 1046 (2001).
- <sup>53</sup>H. Jobic, N. Rosenbach, A. Ghoufi, D. Kolokolov, P. Yot, T. Devic, C. Serre, G. Ferey, and G. Maurin, *Chem. -Eur. J.* **16**, 10337 (2010).
- <sup>54</sup>A. Ghoufi, *Phys. Rev. Mater.* **7**, 126001 (2023).